Journal of Colloid and Interface Science 676 (2024) 1055–1067

Contents lists available at ScienceDirect

Journal of Colloid And Interface Science

journal homepage: www.elsevier.com/locate/jcis

Regular Article

Induced-aggregates in photocatalysis: An unexplored approach to reduce the noble metal co-catalyst content

Enqi Bu [a,b], Xiaowei Chen [a,b], Carlos López-Cartes [c], Antonio Monzón [d], Juan José Delgado [a,b,*]

[a] Departamento de Ciencia de los Materiales, Ingeniería Metalúrgica y Química Inorgánica, Universidad de Cádiz, Spain
[b] Instituto Universitario de Investigación en Microscopía Electrónica y Materiales (IMEYMAT), Universidad de Cádiz, Spain
[c] Departamento de Química Inorgánica, Universidad de Sevilla, Spain
[d] Instituto de Nanociencia y Materiales de Aragón (INMA), CSIC-Universidad de Zaragoza, Spain

GRAPHICAL ABSTRACT

Aggregates created by a simple physical method promote the charge mobility between semiconductor nanoparticles and, combined with the selective photo-deposition of platinum, dramatically improve the hydrogen production when low loadings of Pt are used.

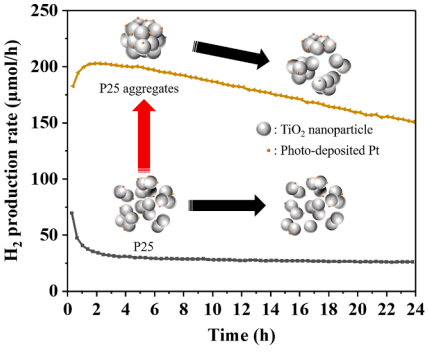

ARTICLE INFO

Keywords:
Ethanol photoreforming
P25
Hydrogen production
Deactivation
Aggregates

ABSTRACT

Photocatalysis has emerged as a promising and environmentally sustainable solution to produce high-purity hydrogen through ethanol photoreforming. It is commonly accepted that adding co-catalysts, especially noble metals, significantly enhances the catalytic activity of semiconductors. However, the high cost of noble metals such as Pt may limit the real application of this emerging technology. Here we evaluate the possibility of reducing the noble metal loading by creating the appropriate interface between pre-formed semiconductor nanoparticles. Commercial titania (P25) was selected as the semiconductor due to its commercial availability, facilitating the straightforward validation and corroboration of our results. Pt was selected as co-catalyst because one of the most efficient photocatalysts for the ethanol photo-reforming is still based on the use of P25 in combination with Pt. We report that the creation of induced aggregates dramatically improves the total hydrogen produced when very low loadings ($\leq$0.05 wt%) of Pt are used. We have developed a pioneering reactor designed for conducting photoluminescence studies under authentic operational conditions of nanoparticle suspensions in the liquid phase. This approach allows us to obtain the average photoluminescence emission from the P25 agglomerates what it would be impossible to obtain by using standard solid samples holders. Thanks to this

* Corresponding author at: Departamento de Ciencia de los Materiales, Ingeniería Metalúrgica y Química Inorgánica, Universidad de Cádiz, Spain.
E-mail address: juanjose.delgado@uca.es (J.J. Delgado).

https://doi.org/10.1016/j.jcis.2024.07.028
Received 30 January 2024; Received in revised form 17 June 2024; Accepted 4 July 2024
Available online 15 July 2024

equipment, we can conclude that this remarkable improvement of the activity is mainly due to creation of an interface that favors the charge transfer between the particles of the aggregates. According to this, the titania nanoparticles of the agglomerates act as an antenna to collect the photons of the sun-light and produce the photo-excited electrons that will be transferred to the platinum nanoparticles located in the same agglomeration. In contrast, raw P25 with low loadings of Pt would have a high number of titania nanoparticles without platinum, and therefore, inactive. This result would be especially relevant in the case of immobilized photocatalytic systems for real future photocatalytic reactors because the immobilization of the semiconductors would generate similar interactions to the one created by our method. Consequently, the initial semiconductor immobilization followed by the subsequent photo-deposition of the co-catalyst emerges as a promising approach for a substantial reduction of the co-catalyst content.

1. Introduction

Hydrogen stands at the forefront of a transformative vision for a greener future, serving as a paramount energy carrier with remarkable potential to revolutionize our world [1]. With its capacity to release energy through clean and efficient combustion, hydrogen offers a compelling alternative to traditional fossil fuels, providing a pathway to drastically reduce greenhouse gas emissions and combat climate change [2]. Embracing hydrogen as a clean energy solution not only promises a more sustainable tomorrow but also holds the key to safeguarding our planet's delicate ecosystems for generations to come. In recent years, sunlight-driven photoreforming has attracted significant attention as a promising alternative approach for overall hydrogen production [3,4]. Generally, the photoreforming hydrogen production is performed in an organic aqueous solution, where the organic compounds can serve as sacrificial agents to promote hydrogen production by consuming photogenerated holes [5]. Plenty of organics have been utilized to facilitate photoreforming hydrogen production, such as methanol [6], ethanol [7], glycerol [8], cellulose [9], etc. In addition, different organic sacrificial agents are also compared to optimize the efficiency of hydrogen production [10,11]. Nevertheless, compared with various types of sacrificial agents, the performance of photocatalyst remains the primary determinant of photocatalytic activity. Therefore, the research and development of novel photocatalysts become the key to further enhance the efficiency of photoreforming hydrogen production.

In ethanol photoreforming, diverse semiconductor-based catalytic systems have been explored with excellent results such as TiO_2, WO_3, ZnO or CdS [12]. However, those materials require a co-catalyst, such as noble metals, to facilitate the charge separation and also catalyze the reduction half reaction. For instance, bare TiO_2 is almost inactive for photoreforming of alcohols, whereas the addition of different loading, up to 5 %, of various noble metals, such as Pt, Pd, Au, Rh, Ag and Ru, improves the H_2 production [12].

Titanium dioxide (TiO_2) is by far the most widely studied material for photocatalytic applications due to several beneficial properties including low cost, non-toxicity, relatively broad light absorption, good photostability and high photocatalytic activity compared to other metal oxides [13]. P25, a commercially available form of TiO_2, is a mixed-phase nanoscale material consisting of approximately 70–80 % anatase, 20–30 % rutile, and a small amount of amorphous phase. This unique combination of phases contributes to its photocatalytic properties, making it an efficient catalyst for various applications, including ethanol photo-reforming for hydrogen production [14,15]. To date, its remarkable efficiency and effectiveness have set the bar for other photocatalysts, serving as the coveted benchmark that researchers strive to surpass [16–18]. On the other hand, numerous research studies have been dedicated to enhancing the photocatalytic activity of P25 through the addition of co-catalysts [19,20] or the creation of heterojunctions [21,22]. Therefore, a comprehensive understanding of the photocatalytic behaviors of P25 is essential for the evaluation and development of photocatalysts. Additionally, the use of P25 has been proposed to perform fundamental research and as a reference material since it is commercially available and, therefore, the results would be easily corroborated by the research community [23,24].

Despite substantial efforts, a thorough understanding of the catalytic behavior of P25 remains challenging due to the complex nature of this photocatalytic system. One of the most commonly accepted mechanism explaining the enhanced photocatalytic activity of mixed-phase TiO_2 was proposed by Bickley in the early 1990 s [25]. It involves electron transfer from anatase to rutile, reducing recombination rates and promoting efficient charge separation. This model was mainly supported on the lower energy conduction bands of rutile relative to anatase. However, Hurum et al. reached to the opposite conclusion based on EPR characterization and they considered that the electrons are transferred from rutile to anatase nanoparticles [26]. What is obvious is that electron mobility between different nanoparticles is occurring and even Emeline et al. compared this phenomenon with the spillover phenomenon [27].

The addition of novel metals, such as Pt, Au, Pd etc, has also been widely explored as a strategy to further enhance the photocatalytic performance of P25 nanoparticles [28,29]. Several studies have demonstrated that the introduction of Pt as a co-catalyst on P25 can significantly improve the reaction rates and overall efficiency in various photocatalytic applications [30,31]. Most of the authors underline the contribution of Pt nanoparticle as electron sink to subsequently overcome the electron-hole recombination limitations of P25 [32]. Furthermore, Pt not only serves as an efficient electron sink but also acts as an active site for the reduction half-reaction where H_2 is produced during photocatalysis, enabling the efficient conversion of protons into hydrogen fuel [33,34]. Consequently, without Pt, although the P25 nanoparticles can efficiently capture light and generate photoinduced electrons, the catalytic reaction for H_2 production cannot occur, leading to a waste of the photo-generated electrons and low efficiencies. For this reason, the metal loading optimization is one of the most critical synthesis points. In this sense, we should consider two different aspects to improve the photocatalytic performance. The first one is the location of the Pt nanoparticles because it is obvious that the most efficient configuration is to have the Pt nanoparticles where the photo-generated electrons would be accumulated. For this reason, photo-deposition is the most preferred synthesis route because the platinum would be selectively deposited where the electrons would naturally accumulate on the sample [35,36]. The second point, which is less discussed, is related to the loading, as mentioned before, requires that all titania nanoparticles or agglomeration of nanoparticles will be decorated with Pt to efficiently utilize all the photo-induced exited electrons. Some authors also reported that too high noble metal loadings can produce a negative effect because these metal nanoparticles would reduce the amount of light that reaches the titania where most of the photo-excited electrons are generated [37].

In this study, we investigate the potential of enhancing electron mobility between nanoparticles through the formation of particle aggregates. Our main focus is to explore how this innovative approach can significantly reduce the required content of co-catalyst, particularly platinum, while keeping exceptional photocatalytic performance in ethanol photoreforming for hydrogen production. As mentioned before, P25 was selected as the semiconductor to facilitate the validation of our results, but we expect that our results will be extended to most of the semiconductors. Pt was selected as co-catalyst because one of the most

efficient photocatalysts for the ethanol photo-reforming is still based on the use of P25 in combination with Pt. However, our findings have broader implications beyond our specific system, as they prompt essential questions about the often-overlooked influence of particle aggregations on photocatalytic activity. Understanding this aspect could play a crucial role in determining the overall photocatalytic performance and cover the way for more efficient and environmentally sustainable photocatalytic applications, contributing to a promising future for green energy technologies.

2. Materials and methods

2.1. Preparation and characterization

The commercial Acros Organics aeroxide P25 was used as the raw photocatalyst in this study. The samples with induced aggregation (IA-P25) were obtained by a simple filtration process. Normally, 250 mg of P25 was suspended in 50 mL of Milli-Q water and stirred for 1 h. Subsequently, it was filtered using a 0.45 μm nylon membrane (Filter-Lab®) and dried in air at 60 °C. Finally, the sample was ground and sieved using a 100 μm sieve. Additionally, several samples with different aggregation sizes were obtained by grinding pellets of P25 that were sieved using a sieve tower. The following particle size fractions were collected: 400–300, 300–200, 200–100 and 100–50 μm.

X-ray diffraction (XRD) patterns were obtained on D8 advance-A25 diffractometer (Bruker) with Cu Kα ($\lambda = 0.154$ nm) radiation source at a scanning rate of 2° min^{-1}. The Brunauer-Emmett-Teller (BET) specific surface area (S_{BET}) was analyzed by nitrogen adsorption–desorption using a Micromeritics ASAP 2020 apparatus. All the samples were degassed at 200 °C for 2 h prior to the measurements. Besides, the Barret-Joyner-Halender (BJH) method was used to determine the pore size distribution.

The morphology and aggregate size of the samples were studied by scanning electron microscopy (SEM) using a Nova NanoSEM 450 at an accelerating voltage of 10 kV with a spatial resolution of 5 nm. In order not to generate new aggregations, a diluted suspension of the sample (10 mg of photocatalysts into a mixed solution of 35 mL ethanol and 35 mL water) was prepared and a few drops were deposited on the aluminum sample holder. High-angle annular dark field scanning transmission electron microscopy (HAADF-STEM) characterization was performed on a Talos F200X instrument. Additional experiments were carried out using an aberration corrected TEM (Titan Themis^3, Thermo Fisher Scientific) to exclude the formation of single atoms sites during the platinum photo-deposition.

Dynamic light scattering (DLS) and laser diffraction (LD) measurements were performed to determine the aggregates sizes of P25 and induced aggregates P25 samples. Due to the expected small size of the aggregates of the P25 sample, a ZetaSizer Nano ZS (Malvern) was used since this equipment is optimized to analyze particles with a size ranged from 10 nm to 10 μm. A MasterSizer 2000E (Malvern) was utilized in the case of the IA since it was adequate to analyze accurately bigger particles between 0.2 and 2000 μm. The results from DLS/LD were compared with SEM measurements to ensure comprehensive characterization of particle size distributions in our study.

UV–Vis diffuse reflectance spectra (DRS) were obtained on a Shimadzu UV-3600i spectrophotometer equipped with an integrating sphere. Conventional XPS (X-ray Photoelectron Spectroscopy) measurements were performed in a Kratos Axis UltraDLD spectrometer (Kratos Analytical Ltd., Manchester, UK) using monochromatized Al Kα ($h\nu = 1486.6$ eV) radiation with a power of 150 W. High-resolution spectra were acquired with a pass energy of 20 eV. Samples were pressed into self-supported pellets and fixed by means of a conductive double-sided carbon polymer tape. Charging effects were compensated with the coaxial charge neutralizer device developed by Kratos, and the binding energy (BE) scale was corrected with respect to adventitious carbon and set to 284.8 eV.

The room temperature photoluminescence (PL) spectra were obtained by a fluorescence spectrometer (Horiba Fluorolog-QM) equipped with a continuous 75 W Xenon arc lamp and a photomultiplier tube (PMT) detector (920IS). Photoluminescence was recorded under the photocatalytic reaction conditions. For this, 10 mg of solid samples were suspended in 70 mL aqueous solution (35 mL water and 35 mL ethanol) and then filled into a high precision cell with stirring for measurement. The excitation wavelength was selected to be 325 nm and the emission scanning from 380-620 nm was collected from the front face. The photon detection efficiency of the PMT detector and the grating was calibrated over the full range of wavelengths used and all the spectra included in this work were corrected using this calibration to prevent error in determining the maximum of the fluorescence emission. All the slit widths were set at 5 nm.

2.2. Photoreforming hydrogen production

The photo-catalytic experiments were conducted using a custom-designed on-line photo-reactor that allows simultaneous measurements for up to four samples (Fig. S1). The light irradiation was provided by a solar simulator with a 450 W Xenon lamp (Oriel Sol3A, Newport). To maintain a constant reactor temperature of 8 °C, we employed a cooling jacket system connected to a thermostatic bath (AP7LR-20, VWR). This cooling system ensured precise temperature control, providing an optimal and stable environment for the photoreforming hydrogen production studies. To verify the stability of the light source during each experiment, we conducted spectrum measurements using a spectrometer (Flame-S, Ocean Insight) before and after each run. A representative spectrum of the light source can be seen in Fig. S2. Additionally, the sun light irradiance was quantified using a pyranometer (LP PYRA 03 AV, Delta Ohm), reaching an intensity of 1.6 sun. Each of the reactor has an illuminated area of 15.2 cm^2.

In a standard photocatalytic test, we dispersed 10 mg of photocatalyst nanoparticles into 70 mL of a 50 % by volume ethanol aqueous solution, which was continuously magnetically stirred at 800 rpm. Before sealing the reactor, we carefully added an appropriate volume (87 μL) of a $Pt(NO_3)_2$ solution (55.6 ppm of Pt) to enable in-situ photodeposition of Pt as a co-catalyst, resulting in a final Pt loading of 0.05 wt%. After conducting a leak test to ensure a sealed environment, any residual air within the reactor was effectively removed by purging with argon at a flow rate of 15 mL/min for 2 h. Throughout the experiments, this flow of argon was maintained serving as a carrier to transport the reaction products for analysis by an on-line gas chromatograph (GC Trace 1300, Thermo Scientific) equipped with a high-sensitivity thermal conductivity detector and a Carboxen 1010 PLOT Capillary GC Column. After 24 h, the photocatalytic tests were stopped, and the samples were collected by filtration and washed carefully with water and then dried at 60 °C. An inductively coupled plasma-optical emission spectrometer (ICP-OES, Spectrogreen FMD46) was utilized to determine the real Pt content of samples post-reaction. Prior to analysis, solid samples underwent chemical acid digestion using a Digiprep JR (SCP-SCIENCE) digestor. The Pt loading of all samples included in this study is summarized in Table S1 and, in all cases, was close to the theoretical loading. The analysis of intermediates in the liquid phase was performed at the end of the photocatalytic test by High Performance Liquid Chromatography (HPLC, Thermo Scientific Dionex UltiMate 3000). An HyperREZ XP Organic Acid Bum column (100x7.7 mm), utilizing a 0.005 N sulfuric acid in water as mobile phase, was employed with a flow rate of 0.5 mL/min. The column was maintained at a temperature of 25 °C, and the injection volume for each sample was set to 10 μL.

2.3. Photocatalytic degradation

Methylene blue (MB) degradation experiments were conducted at room temperature using the same irradiation system. Typically, 10 mg of samples were suspended in 50 mL of MB aqueous solution (10 mg/L)

with stirring. Before initiating the photocatalysis, the reactor was kept in the dark for 20 min to reach adsorption–desorption equilibrium. The solution was then sampled every 5 min and subjected to centrifugation for analysis. The concentration of supernatant was measured at 665 nm using a Shimadzu UV-3600i spectrophotometer, and the activity was determined by C_t/C_0, where C_t is the concentration at each time interval and C_0 is the initial concentration.

3. Results and discussion

3.1. Characterization

As mentioned in the introduction and the experimental sections, a soft process to induce the formation of aggregates was selected to not modify the structural and superficial properties of the P25. To verify this, XRD diffractograms and XPS spectra of both fresh and agglomerated samples were carried out. As shown in Fig. S3, P25 and IA-P25 displayed almost identical diffraction peaks. The characteristic diffraction peaks at 25.3°, 37.8°, 48.0°, 53.9° and 55.1° were corresponding to (101), (004), (200), (105) and (211) planes of anatase (JCPDS 99–0008), whereas the peaks at 27.4°, 36.1°, 41.2°, 54.3° and 56.6° were corresponding to (110), (101), (111), (211) and (220) planes of rutile (JCPDS 99–0090), respectively. In addition, the crystallite sizes (Table 1) were estimated by the Scherrer formula (Formula S1), which indicated that the treatment has no effect on the crystallites of anatase and rutile in P25. In both samples, the proportions of anatase and rutile were estimated to be approximately 84 % and 16 %, respectively.

Fig. S4 shows the high resolution XPS spectra of P25 and IA-P25. No obvious differences can be observed between the spectra of both samples. Ti $2p_{3/2}$ and $2p_{1/2}$ XPS peaks are centered at binding energies of 458.7 and 464.4 eV, which are typical of Ti^{4+}-O bonds in TiO_2 [38]. The high-resolution O 1 s spectra show two peaks at approximately 529.9 and 531.6 eV, which can be attributed to the Ti^{4+}-O bond and surface hydroxyl groups (Ti-OH bonds), respectively. The contribution of hydroxyl groups to the spectra area is 15 % of the total in both cases. These results clearly indicate that the process used to obtain the particle aggregation of P25 does not modify the sample.

However, slightly modifications of the textural properties were observed due to the particle agglomeration. Fig. 1 illustrates the nitrogen adsorption–desorption isotherms and pore size distributions of P25 and IA-P25. It could be seen that both samples showed type IV isotherms with a type H3 hysteresis loop (IUPAC classification) at high relative pressure, indicating the existence of mesopores (2–50 nm) [39]. Besides, an hysteresis was observed in both cases at high P/P_0, suggesting the presence of macropores (>50 nm) [40]. Considering that commercial P25 is produced through the hydrolysis of $TiCl_4$ in a hydrogen flame, the formation of pore structures in P25 and IA-P25 could be attributed to the aggregation of TiO_2 crystallites [41]. From the pore size distributions (Fig. 1 inset), an obvious increase in the pore volume of large pores (20–50 nm) could be observed in IA-P25. Moreover, compared with the raw P25, the specific surface area (Table 1) of IA-P25 slightly decreased, while the pore volume and average pore size approximately doubled. These textural changes are in good concordance with the formation particle aggregations after the treatment [42].

To further characterize the aggregates and quantify their size, the samples of P25 and IA-P25 were dispersed in solution under the same conditions as photocatalytic experiment and then studied by SEM. From the images shown in Fig. 2, it is obvious that the particle aggregation was significantly more evident in the IA-P25 sample. 250 aggregates were randomly selected from SEM images of P25 and IA-P25, and their sizes were measured. The corresponding size distribution is shown in Fig. 2c,f. According to the analysis, the average aggregate size of IA-P25 was 35.4 ± 2.1 μm, which was about 10 times the aggregate size of P25 (3.5 ± 0.1 μm).

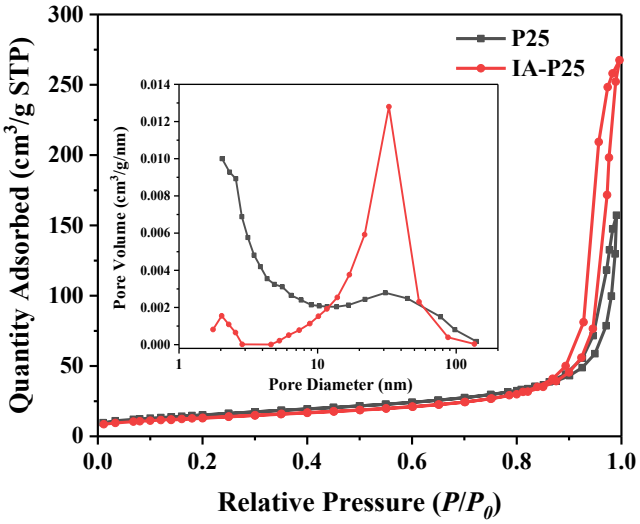

Fig. 1. N_2 adsorption–desorption isotherms and pore size distribution curves (inset) of P25 and IA-P25.

Particle size distribution was also obtained by DLS/LD technique, which offers several advantages. The main one is that it measures particles in suspension rather than in dry powder, providing a more accurate view of particle aggregation in the reaction environment. Moreover, it facilitates analysis of a larger number of particles, enhancing the comprehensiveness of our data. In comparison, SEM measurements may underestimate the presence of small nanoparticles due to the fact that the magnification needed to observe small and big agglomerations is different. Moreover, SEM sample preparation, involving suspension of nanoparticles, deposition on a holder, and evaporation, can induce additional aggregation, particularly affecting smaller sizes that will be underestimated. However, DLS/LD and SEM results were largely consistent and show the dramatic change in the aggregates sizes. The results obtained for P25 via DLS/LD fell within the expected range of 175–300 nm reported in literature, although larger aggregations up to approximately 1 μm were observed, likely influenced by the absence of ultrasound in sample preparation to prevent aggregation structures [43,44]. In the case of IA-P25, DLS/LD identified distinct peaks around 0.8, 10, and 50 μm, aligning closely with SEM results while offering greater accuracy in quantifying smaller particles that SEM had underestimated. These results indicate that we managed to create particle aggregation through a very simple and reproducible method that also preserves the chemical and structural characteristics of P25.

UV–Vis DRS spectra of P25 and IA-P25 were measured to investigate their optical absorption properties. As shown in Fig. S5, both samples displayed very similar reflectance curves with absorption edges at ca. 410 nm. Furthermore, the band gap energies were calculated according to the Kubelka-Munk method (Formula S2 and Fig. S5 inset). The band gaps of P25 and IA-P25 were estimated to be 3.11 and 3.14 eV, respectively, which were comparable to the values previously reported in the literature [45]. Since the absorption properties can be easily modified by superficial changes of anatase/rutile ratio [26], the similarities in the optical properties of the samples also demonstrate that the employed method did not significantly affect the main properties of P25.

Table 1
Characteristic parameters of P25 and IA-P25.

sample	XRD		N_2 adsorption–desorption			UV–Vis
	Crystallite size (nm)		S_{BET} (m^2/g)	Pore volume (cm^3/g)	Pore size (nm)	Band gap (eV)
	Anatase	Rutile				
P25	21.3	37.9	55	0.2	17.9	3.11
IA-P25	21.6	36.3	47	0.4	29.9	3.14

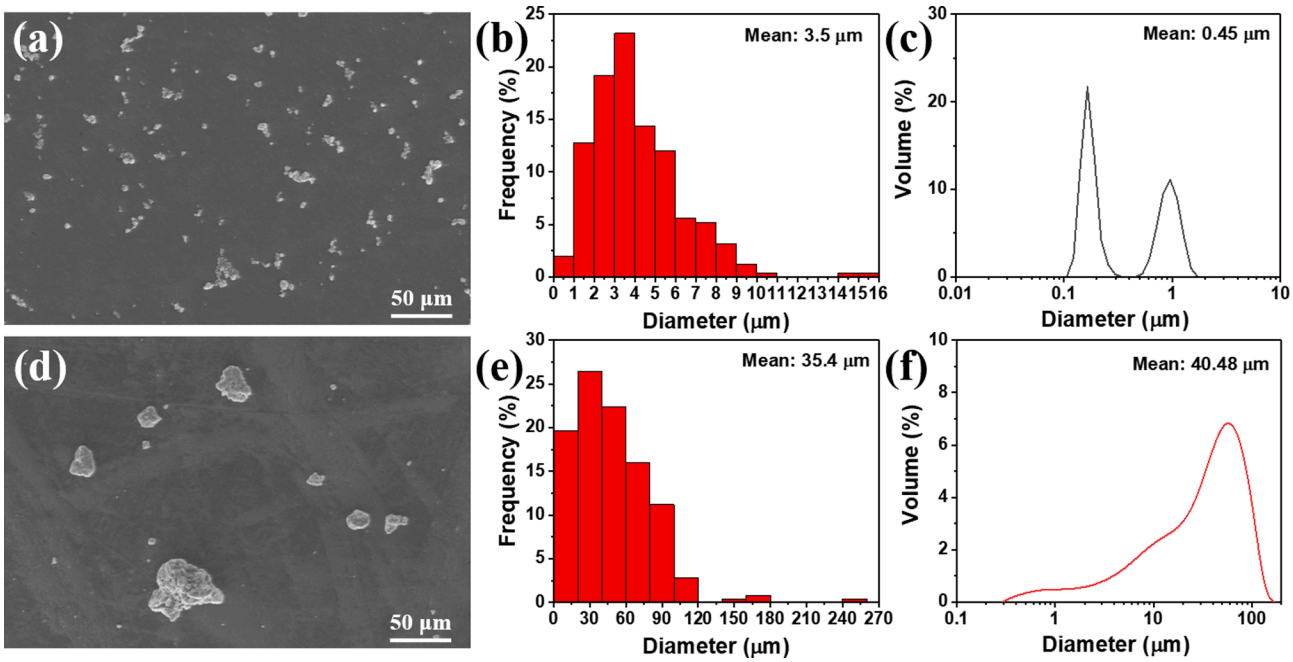

Fig. 2. Low magnification SEM image, particle size distribution using SEM images and DLS/LD technique of P25 (a, b and c) and IAP25 (d, e and f).

So, the singular photoactivity properties of the IA-P25 can univocally be attributed to the formation of particle aggregation.

3.2. *Photoreforming hydrogen production*

The ethanol photoreforming hydrogen production via P25 and IA-P25 was carried out to evaluate the effect of particle agglomeration on the photocatalytic performance when low co-catalyst loading is used. Fig. 3a shows the results of photocatalytic tests using both samples with a platinum loading of 0.05 wt%. It could be observed that the H_2 rate of P25 exhibited an initial reaction rate of 69.7 μmol/h that rapidly decreased to 37.6 μ mol/h after one hour. Finally, the activity slowly decreased to a relatively stable value of 26.1 μ mol/h. The deactivation in this kind of reaction using low metal loadings has been previously attributed to the interaction of Pt atoms and oxygen vacancies [23]. Besides, the constant accumulation of intermediates during the photocatalytic reaction and their irreversible adsorption on the Pt surface have also been considered to be one of the causes of deactivation [46]. It is commonly accepted that the reduction half-reaction would take place on the surface of the co-catalyst, which in our case is platinum, while the oxidation half-reaction occurs on the surface of TiO_2 to form the corresponding oxygenated intermediates. Among them, acetaldehyde was recognized as the main intermediate in the liquid phase, followed by acetic acid [47]. The analysis by HPLC of the liquid phase after reaction allowed us to determine the presence of acetaldehyde, acetic acid and formic acid (Fig. S6). The concentration of acetaldehyde was approximately twice that of acetic acid. Small amounts of formic acid were also found in the reaction solution, and it should be pointed out that Huang et al. recently demonstrated that trace amounts of formic acid, even below the detection limits of standard analysis methods, could be highly toxic to Pt co-catalyst [48].

Fig. 3a also shows that the induced particle agglomeration in IA-P25 resulted in a remarkable enhancement of its photocatalytic activity, showing an initial activity up to 3.5 times higher than that of the conventional P25. Furthermore, the reaction evolution of IA-P25 exhibited notable differences compared to P25. The H_2 production rate of IA-P25 reached a maximum value of 234.7 μ mol/h at a reaction time of 1 h, but subsequently, the H_2 production rate exhibited a slow decrease, resulting in an overall activity loss of 57 %. This result was further validated through repeated experiments using different batches of IA-P25 (Fig. S7). According to the above discussed catalyst characterization results, the main difference between P25 and IA-P25 was the size of

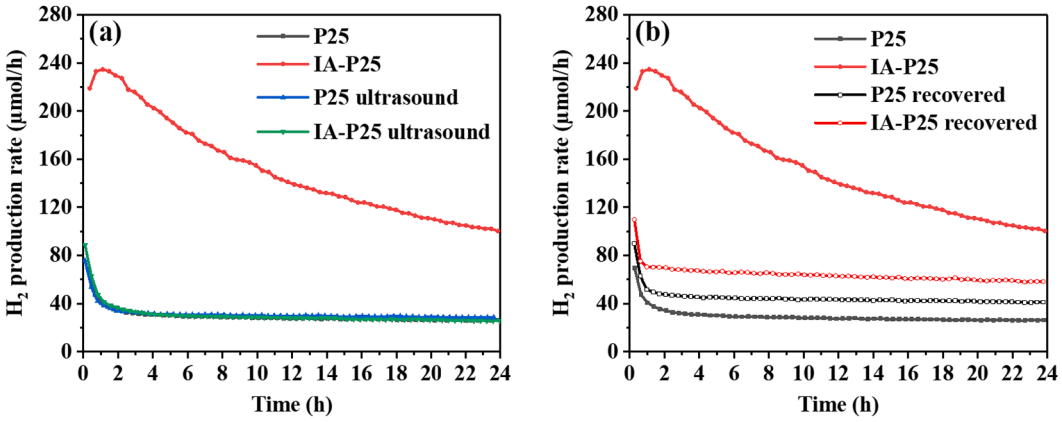

Fig. 3. Photocatalytic hydrogen production rate of (a) P25 and IA-P25 samples with and without ultrasound treatment, (b) P25, IA-P25 and their recovered samples.

aggregates before photocatalysis rather than any other properties, which preliminarily indicated that the existence of larger aggregate was the origin of this significant improvement of the hydrogen production rate. Besides, the platinum particle size of the samples must be evaluated since it is a parameter that may also strongly affect the photocatalytic mechanism and the activity [49]. For this purpose, the platinum particle size distribution of the most relevant samples after reaction was obtained by HAADF-STEM images, which are included in Fig. S8. Surprisingly, it can be observed that the Pt size on IA-P25 was even slightly larger than that found on P25. However, according to recent theoretical calculations, the photocatalytic properties are boosted by decreasing the Pt size, as it promotes the photoelectron transfer [50]. Thus, the enhanced catalytic activity observed in IA-P25 cannot be attributed to differences in the particle size of Pt. Furthermore, considering that the metal loading is the same for both samples and the particle size is slightly larger in the case of IA-P25, it is logical to assume that there are fewer Pt particles on the surface of this sample. This observation may indicate a reduction in available catalytic actives sites for the protons reduction half-reaction, which is considered as the limiting step in several studies [51,52].

Finally, and despite the limitations of TEM related to the very small area that it can be analyzed, it should be pointed out that the agglomerations of titania nanoparticles without Pt were more frequent to be observed in the P25 sample compared to the IA-P25. This is logic if we also consider the huge difference in the size of the agglomerations that it was previously discussed.

In order to fully corroborate that the improvement of the catalytic activity is a result of the particle aggregation, additional experiments were carried out applying low-intensity ultrasound (US) treatment to the samples before the photocatalytic tests for 2 min using a VEVOR ultrasonic cleaner (40 kHz, 120 W). US is commonly used in the literature to efficiently disperse nanoparticles in liquids and to break weak interaction between nanoparticles, as we used in the aggregate induction process. According to the literature, US treatments may also induce the formation of oxygen vacancies on the TiO_2 surface and improve the photoactivity [53,54]. To confirm that the applied US treatment did not modify the properties of the raw P25, this sample was also exposed to US. As shown in Fig. 3a, both the raw P25 and the IA-P25 after US treatment exhibited comparable activity, similar to that of the P25 without US treatment. Therefore, it can be concluded that the employed low-intensity ultrasound method only dispersed the aggregates without modifying the photocatalyst itself, further verifying the importance of particle aggregations. Moreover, the average Pt particle size (~1.34 nm) measured from TEM images (Fig. S8c) in the case of the sample IA-P25-0.05Pt with an ultrasound treatment was very close to that of P25-0.05Pt, which matches well with the aforementioned results and also supports the idea that particle aggregations promote the accumulation of photo-excited electrons on same regions of the TiO_2 surface, resulting in fewer Pt particles with a slightly larger volume.

After clearly demonstrating the benefits of TiO_2 aggregates, it is of great interest to evaluate their stability under reaction conditions, which could also provide a suitable explanation for the severe deactivation. During the photocatalytic experiments, the aggregates were subjected to intensive magnetic stirring (800 r.p.m.) for 24 h, which could affect the cohesion between the particles of the aggregates. The aggregate size distribution was determined from SEM images and DLS/LD of P25 and IA-P25 after photocatalytic tests (Fig. S9). The DLS/LD results show small differences between the fresh and the spent P25 catalyst. The contribution of the fraction of aggregates observed in the P25 sample at around 1 μm became less relevant, and the size decreased below 0.60 μm, with the average aggregate size shifting down to 0.27 μm. However, the average size of the aggregates in IA-P25 dramatically decreased from approximately 40.5 μm to 12.9 μm. This suggests that the TiO_2 aggregates in IA-P25 are not stable under reaction conditions. In fact, we can consider that the original aggregates disaggregate, producing new aggregates of around 10 μm that are relatively stable since remain even after 24 h of reactions. However, the fraction of particles below 1 μm is also higher, which could indicate that over time, the 10 μm aggregates may also collapse.

Recovery tests were conducted using both P25 and IA-P25 samples to further investigate the stability of the aggregates. After completing several standard 24 h experiments, the photocatalysts were filtered and dried at 60 °C. It is clear that there are significant similarities between this recovery method and the procedure used to generate aggregates in the IA-P25 sample. Consequently, we can expect that similar aggregates to those observed in IA-P25 would be formed in the recovered P25 sample. Interestingly, despite the presence of the same aggregates, the photocatalytic performance of the recovered P25 sample was observed to be slightly higher than that of the raw P25 but significantly lower than that of IA-P25 (see Fig. 3b). To fully understand these results, we must consider that there is a critical difference between both samples: in the recovered samples, the Pt was already present before aggregate formation, resulting in a random distribution of Pt within the aggregates. This differs from the situation when the aggregates are formed before platinum photo-deposition because, in the latter case, the Pt nanoparticles will be anchored where the photo-excited electrons accumulate, while in the former case, this will not happen, and only statistics will govern this possibility. For this reason, the improvement in the recovered P25 is limited. Therefore, we can conclude that the impact of aggregation on various aspects such as light dispersion and absorption is not responsible for the photocatalytic improvement. Even more, this provides clear evidence of electron mobility between different titania nanoparticles within the same aggregate, strongly influencing the distribution of electrons among nanoparticles. In the case of the recovered IA-P25, we observed much lower H_2 production rate than IA-P25, what it can be understood due to the rearrangement of the initial aggregates during the recovery process. However, the activity of this sample is still higher to the obtained for the raw and recovered P25, indicating that some of the aggregates of the IA-P25 persist after the recovery process, maintaining an optimal distribution of Pt.

In order to exhaustively investigate the effect of stirring on the aggregate stability, we conducted two additional experiments with the IA-P25 sample. In these experiments, the IA-P25 sample underwent a one-hour illumination period, followed by a 24-hour dark period, and then illumination was resumed. The crucial variation between these experiments was the stirring conditions: in one case, stirring was paused during the dark period to prevent disaggregation, while in the other case, stirring was maintained throughout the process. The results of these experiments, as depicted in Fig. 4, provided compelling evidence of the dominant influence of disaggregation on the deactivation behavior of IA-P25. Initially, both samples exhibited nearly identical

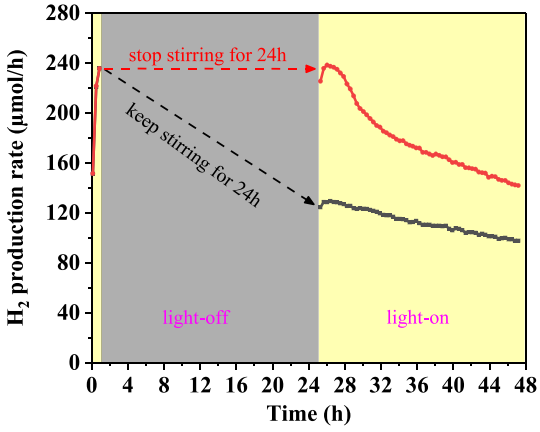

Fig. 4. Photocatalytic hydrogen production rate of IA-P25 under different treatments: stop (red line) or keep (black line) the stirring during 24 h of darkness period. (For interpretation of the references to colour in this figure legend, the reader is referred to the web version of this article.)

activity before the cessation of light, indicating their similar characteristics at this point. The sample subjected to no stirring during the dark period (red line) showed minimal change in activity after the dark period, closely resembling the behavior observed during a standard photocatalytic experiment with IA-P25. In contrast, when stirring was maintained throughout the darkness period (black line), the resumed hydrogen production rate decreased dramatically by 48 % compared to before the dark period. This experiment effectively demonstrated that the disaggregation of aggregates predominates the deactivation behavior observed in IA-P25 samples. The clear distinction in activity between the continuously stirred and non-stirred samples underscores the critical role of aggregate stability in maintaining photocatalytic activity.

To determine the effect of stirring the samples before the platinum photodeposition on the photocatalytic activity, the raw P25 and the IA-P25 samples were stirred for 24 h prior to photocatalysis using the same amount of water (35 mL) required for the photocatalytic test. Afterward, the ethanol (35 mL) was added and the standard experiment, including the Pt photodeposition, was started. As seen from Fig. 5, the stirring treatment did not affect the activity of P25, which is consistent with the previous results obtained using the US and suggests that no large aggregates are present in the raw P25. In contrast, the catalytic performance of the IA-P25 is strongly affected by this stirring treatment. The sample exhibited an initial H_2 rate of 182.8 μ mol/h, which was slightly lower than that observed for IA-P25 (218.9 μ mol/h). However, what it is more notable is that the deactivation was less pronounced than that of the original sample. In fact, the deactivation was less than 25.6 % of the maximum H_2 production rate after 24 h. Moreover, the stirred sample showed higher performance after about 4 h of illumination than the IA-P25. In fact, when considering the total green hydrogen produced during the photocatalytic tests (Fig. S10), the amount obtained with the pre-stirred IA-P25 was 1.2 times higher than that of IA-P25 and 6.2 times higher than that of P25. It should be mentioned that the average size of Pt in this case was 1.6 nm (Fig. S8d), which falls between the values of IA-P25 (1.7 nm) and the P25 (1.4 nm), thus proving again that the platinum nanoparticles itself cannot explain the photocatalytic activity.

Based on the previously discussed results, it can be concluded that the deactivation of IA-P25 was mainly due to the separation of the particles forming aggregates during the reaction. Additionally, if we consider that the catalytic activity of stirred IA-P25 was higher than that of the raw sample and the intermediates at the end of the reaction were similar (Fig. S11), it can be concluded that photocatalyst poisoning by reaction intermediates is not the main cause of deactivation. However, considering the very low loading of platinum, it cannot be excluded that its contribution to the deactivation of the sample when the aggregates size was stabilized.

To in depth study the effect of the aggregates on the photocatalytic activity, a series of P25 with different initial aggregate sizes were prepared and subjected to photocatalytic experiments. We can observe in Fig. 6 that all the fractions show a similar shape and that after the maximum we can observe a continues deactivation. The lowest photocatalytic activity was obtained for the sample with the biggest agglomeration of P25 particles and the optimum was observed for the sample with aggregates between 50 and 100 μm. It is reasonable to assume that as the size of the aggregates increases, the shadow effect experienced by its core particles will also be more significant. Therefore, too big aggregates (>100 μm) will not be the best approach to efficiently exploit the irradiated light since the particles in the outer part of the aggregates will absorb part of the incident radiation, while less radiation would be available for the inner samples.

Although the observed dramatic improvement in photocatalytic activity is associated with agglomeration of the particles, it is reasonable to wonder about the underlying factors. An important aspect to be considered is how the photo-deposited platinum nanoparticles are distributed in the titania support. Therefore, it was of interest to study the effect of Pt loadings on P25 and IA-P25. As shown in Fig. 7, the H_2 production rate of both semiconductor supports increased with increasing Pt loading ranging from 0.025 to 0.2 wt%. In the case of P25, the H_2 rate curve of P25-0.025Pt displayed the same trend as P25-0.05Pt, with a relevant decay of activity from the beginning. However, this abrupt deactivation could not be observed when the amount of Pt was higher than 0.05 wt%. A similar behavior has been previously reported by Haselmann and Eder, who observed that samples with low Pt to oxygen vacancies ratios experience fast deactivation at the early stage of the catalytic tests using methanol as sacrificial agent [23]. The authors suggested that the utilization of a small quantity of Pt leads to a reaction mechanism that yields a significant amount of CO. This CO is subsequently irreversibly adsorbed onto the Pt nanoparticles, causing deactivation of the catalyst. Interestingly, this severe deactivation is not observed when utilizing the sample with induced aggregations. Therefore, the use of induced aggregation appears to mitigate this deactivation process, possibly by inducing an alternative reaction mechanism similar to the observed for high loadings in the case of the P25. It is important to note that further studies are required to confirm this hypothesis. In the case of the samples P25 with Pt loadings higher than 0.05 wt% and for all the induced aggregates samples, the H_2 production rate reached its maximum at around 1 h and then gradually decreased. This deactivation rate was smaller with the increase of Pt loading and more severe for IA-P25, probably due to the disaggregation of IA-P25 sample. However, the most relevant conclusion from this study is that the observed improvement in the catalytic activity when using IA-P25 is smaller at higher metal loadings. In fact, the H_2 production rate of IA-

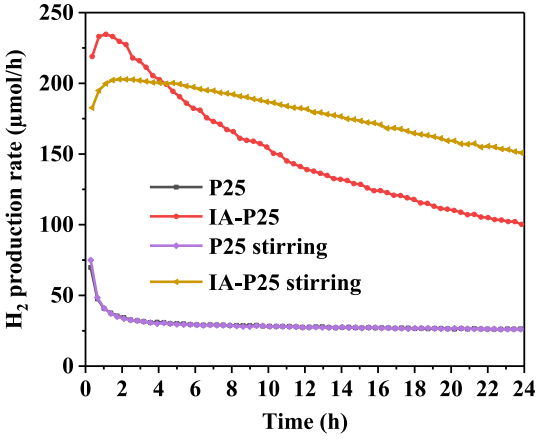

Fig. 5. Photocatalytic hydrogen production rate of samples with and without stirring treatment.

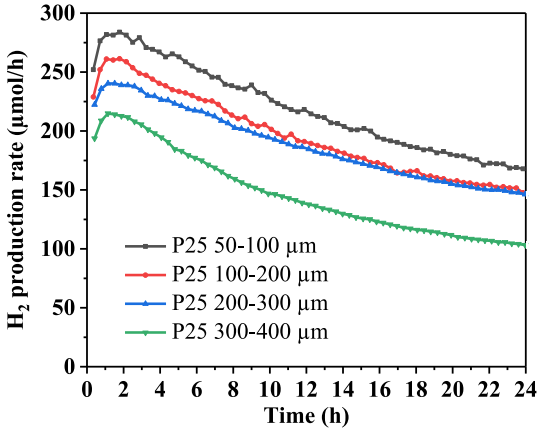

Fig. 6. Photocatalytic hydrogen production rate of P25 fragment with different aggregation sizes.

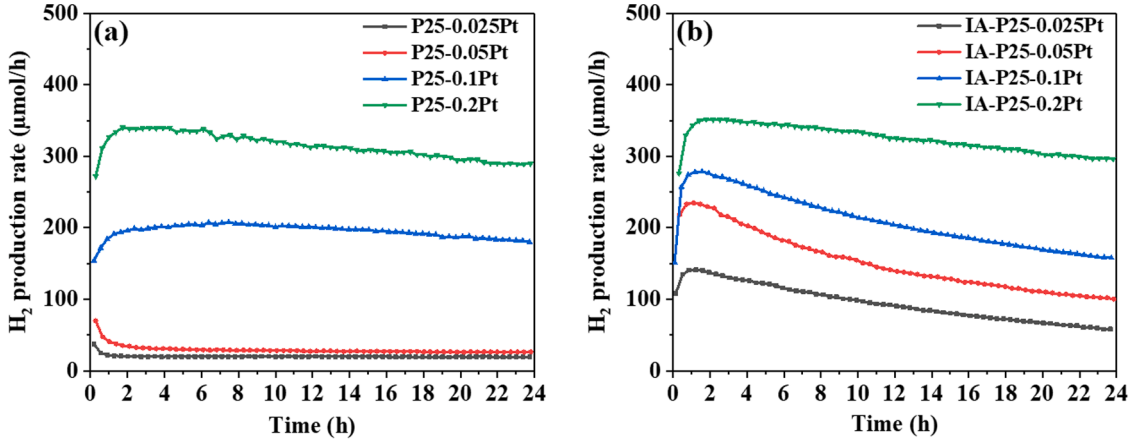

Fig. 7. Photocatalytic hydrogen production rate over (a) P25 and (b) IA-P25 with different amounts of Pt.

P25-0.2Pt was only approximately 4 % higher than that of P25-0.2Pt, and the size of Pt after the reaction was also similar (Fig. S8e, f). Therefore, the improvement of photocatalytic performance resulting from the aggregation of TiO_2 particles is more prominent at very low Pt content. At high Pt content, the similarity of photocatalytic activity on the two supports, as well as the similarity of Pt particle size, suggest that the aggregation mainly optimizes the distribution of Pt on the P25 surface, facilitating electron transfer from the semiconductor to the cocatalyst. It should be noted that HR-HAADF-STEM was also performed using an aberration-corrected electron microscope (Titan Themis Cube) to exclude the possibility of the formation of platinum single atom sites, especially in the case of low platinum loadings. Fig. S8 (i-k) shows representative images of IA-P25-0.05Pt, P25-0.05Pt, and P25-0.025Pt. Although the Pt nanoparticles show atomic resolution, no contrast on the supports was observed that could be related to the presence of single atoms in any of the samples.

To confirm this hypothesis and learn more about the effect of the aggregations on the photocatalytic properties of P25, additional photocatalytic tests of the degradation of MB were carried out over P25 and IA-P25. Unlike photocatalytic hydrogen production, this reaction does not require a co-catalyst and therefore we will be able to exclude the contribution of Pt deposition [55]. As shown in Fig. S12, P25 photodegraded nearly 95 % of MB after 20 min, while IA-P25 only photodegraded about 73 % at the same time. Interestingly, this observation is completely opposite to that obtained from the photo-reforming of ethanol, which demonstrated that the formation of aggregations on P25 has a negative impact on the reaction. This result is in good concordance with the experiments included in Fig. 6, which already demonstrated that the particle aggregation negatively affects the light absorption by titania, which was the main factor causing lower efficiency of photocatalytic degradation. Therefore, as previously mentioned, the key to photocatalytic improvement lies in the optimal deposition of Pt on the support, which allows for an improved number of photo-excited electrons to reach co-catalyst particles and enhance the proton reduction to molecular hydrogen reaction.

3.3. Mechanistic study

At this point, it is of interest to summarize the main observations of our study:

1. Although the formation of particle agglomeration improves the photo-reforming of ethanol, the activity is worse in the case of the degradation of methylene blue.
2. Larger sizes lead to less active photocatalytic systems, probably due to decreased light exposure of particles located in the inner parts of the aggregates.
3. In ethanol photoreforming, the improvement in activity due to particle agglomeration becomes smaller as the cocatalyst (Pt) loading increases.
4. The platinum particle size is very similar in all the cases, ranging from 1.3 nm to 1.7 nm. In the case of low loading photocatalysts, the platinum particle size is slightly larger in samples with agglomerated P25 particles (IA-P25).
5. Many TiO_2 particles or agglomerations in the raw P25 sample with low Pt loadings are not decorated with particles of the co-catalyst.
6. The induced aggregated samples commonly experience continuous deactivation, which can be attributed to the fragmentation of big particles aggregates.
7. Our catalytic tests using raw P25 without platinum produced hydrogen below the detection limit of our photocatalytic reactor.

To propose a suitable model that would explain our results, it would be worth to previously remember the mechanism of the photo-reforming of ethanol. It is commonly accepted that after photo-induced electrons are generated, they move to the Pt nanoparticles, which act as both electron sinks and catalytic centers for the reduction of protons to molecular hydrogen [56,57]. Therefore, those TiO_2 particles without Pt will not have the capability to produce hydrogen due to the rapid charge recombination and the low rate of the reduction half-reaction. As previously mentioned, from TEM images it was shown that TiO_2 particles without Pt were more frequently observed in P25 when low Pt loadings (<0.2 wt%) were used. This is the main reason why photoactivity increases when the Pt loading is higher. Considering that electrons and holes can move between TiO_2 particles, it is clear that the induction of aggregation reduces the number of Pt particles required. In other words, in the presence of the same content of Pt, the formation of aggregates enables more TiO_2 particles or their aggregates to obtain at least one Pt particle, resulting in higher hydrogen production efficiency. Fig. 8a illustrates this idea. During the photodeposition step, as the suspension of P25 or IA-P25 containing the platinum precursor was exposed to the light beam, Pt^{2+} was reduced by photogenerated electrons and subsequently deposited onto the surface of the photocatalyst. When relatively low amount of Pt^{2+} is used (e.g. 0.05 wt%), it is reasonable to assume that Pt will not be deposited on all the particles or small aggregates in P25. In contrast, the formation of larger aggregates in IA-P25 would be beneficial to reduce the required number of Pt particles necessary to ensure that all aggregates would have at least one Pt particle as an active site for hydrogen production, so that photogenerated electrons are not wasted in other undesirable processes such as fluorescence. It is also

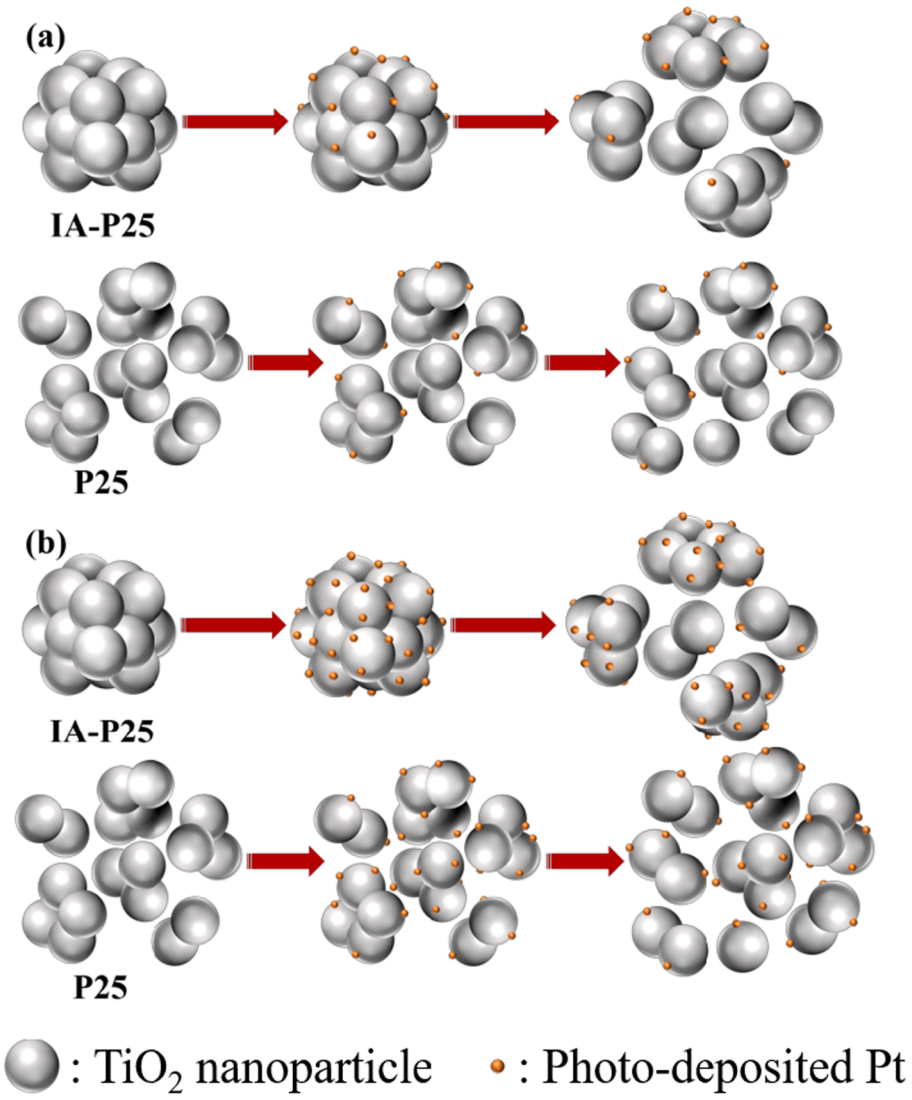

Fig. 8. The proposed mechanism for the improvement and deactivation over samples with (a) lower amount of Pt and (b) higher amount of Pt.

worth noting that photo-deposition method optimizes the photocatalyst synthesis since the Pt is strategically placed in regions of the support where the electrons are located or accumulated. According to this, the aggregates act as antennas to collect the photons that generate excited electrons and holes. The electrons would be able to migrate between nanoparticles to the Pt that are precisely located where the electrons accumulate and would catalyze the reduction half reaction. Simultaneously, the holes move to the titania surface where the oxidation half reaction takes place. This proposed approach offers a straightforward method to maximize the utilization of photoinduced electrons in the reaction, with minimal platinum loading required. This mechanism model also elucidates that the disaggregation of particles agglomerates during the reaction negatively impacts the hydrogen production. As the reaction progresses, the disaggregation generates smaller clusters of titania nanoparticles. In such cases, not all aggregates contain Pt due to limited Pt availability, causing those aggregates lacking Pt to contribute minimally to hydrogen production. When higher amounts of Pt are present, as depicted in Fig. 8b, the Pt was sufficient to be distributed to all aggregates with enough Pt nanoparticles, which prevented the existence of bare semiconductor during the reaction. As a result, little difference can be observed between P25 and IA-P25. Additionally, since most of the clusters formed by the disaggregation of the original aggregates will also have Pt, the deactivation will be more related to the irreversible adsorption of some reaction intermediates or products on the active Pt sites [58].

Obviously, the model described previously is a simplification to make easy understanding. It is more accurate to refer to an optimal amount of Pt nanoparticles, rather than suggesting that a single Pt nanoparticle can be solely responsible for providing activity to the entire aggregate. This is evident when the Pt loading is increased in IA samples, where all aggregates have Pt nanoparticles and the amount of Pt increases, leading to improved photocatalytic performance. However, this improvement is less dramatic than in standard P25 samples. Recently, Qin et al. [59] demonstrated that low loadings of Pt single atoms deposited on anatase TiO_2 thin films are sufficient to achieve a maximized H_2 production rate. The authors concluded that electron diffusion in a semiconductor strongly depends on semiconductor characteristics such as impurities, defects, and crystallinity. When electron diffusion in the semiconductor is poor, a higher concentration of co-catalyst, such as Pt, is required to achieve an optimal photocatalyst. In our case, aggregation formation has improved electron mobility and consequently reduced the amount of Pt sites needed to achieve a maximized H_2 production rate.

It is worth noting that Elser et al. have reported that the nanoparticles aggregation formed by drying a water suspension of P25 improves the reducibility of titania and the generation of electron centers

that are susceptible of adsorbing molecules [60]. They also conclude that this interaction favors the delocalization of photo-induced charges between nanoparticles. While the concept of electron transfer between nanoparticles of a physical induced aggregate is generally not emphasized in photocatalysis studies, it is notable that transient photocurrent experiments often involve sample deposition onto the electrode via drying an ethanol suspension of the raw photocatalyst [61,62]. In this case, it is obvious that the photogenerated electrons need to be transferred from one nanoparticle to another before reaching the electrode [63,64]. It is clear that physical contact between nanoparticles is not the most efficient mechanism of charge transfer, and that the use of conductive binders such as Nafion would improve it. This approach is commonly used for the synthesis of photoactive thin films, although in this case the surface of the photocatalyst would be at least partially covered by this binder and modify its reactivity. More recently, the use of porous single-crystal-based inorganic semiconductor photocatalysts has emerged as probably the most appealing and efficient approach to improve the charge transfer and the photocatalytic activity [65]. However, it should be pointed that our method to improve the charge transfer is really simple and almost universal.

To corroborate the samples P25 with low loading of Pt were intensely studied by HAADF-STEM technique to determine if the aggregates were often without Pt nanoparticles. Analysis of 30 aggregates from the P25 sample with 0.025 % Pt revealed that 19 had no platinum, 6 had fewer than 3 nanoparticles, and 8 had a large number of Pt nanoparticles (an average of 78). This also indicates that probably depending on the interaction between the titania nanoparticles in the support, some aggregates are much more efficient than other and therefore more Pt nanoparticles are deposited on them. Fig. S13 illustrates this study. It must be mentioned, that for IA-P25 sample with the same platinum loading, all aggregates larger than 1 μm are covered by Pt nanoparticles, while only some of those smaller and apparently produced by the disintegration of larger aggregates lack Pt nanoparticles.

PL was used to give further evidence to support the above proposed mechanism and demonstrate the electron transfer between titania nanoparticles. This technique could provide detailed information about the efficiency of charge carrier trapping and recombination in our photocatalysts since the PL emission is produced by the recombination of free charge carriers [66]. Since we want to elucidate the effect of the aggregations, we should skip the use of pellets in this analysis because we would be creating this contact between the nanoparticles even in the raw P25. For this reason, we developed an experimental system that allows to study particles suspensions using the same aqueous solution that it was employed in the reaction (50 % ethanol in water). Analyzing nanoparticle suspensions presents a notable challenge due to the continuous movement of nanoparticles caused by constant stirring. Consequently, the illuminated count of suspended nanoparticles may vary over time. To address this concern, we excited samples IA-P25 and P25 using a wavelength of 325 nm and the emission at 500 nm over a duration of 600 s was recorded (Fig. S14). Notably, the emission remains remarkably stable in both cases, ensuring the acquisition of reliable spectra under these conditions. As shown in Fig. 9a, P25 displayed an emission peak at ~ 500 nm under 325 nm excitation. By contrast, a similar peak with much lower PL intensity can be observed for sample IA-P25, which indicated the lower charge recombination efficiency of IA-P25 since the fluorescence intensity would decline in accordance to a reduction of the charge carrier recombination rate [67]. In addition, the effect of the stirring and ultrasound pretreatment on the PL was also studied to try to correlate them with the photocatalytic activity previously discussed. It could be seen from Fig. 9b that the PL intensity of IA-P25 constantly increased during the 24 h of stirring, while the PL spectrum of P25 remained constant after 24 h (Fig. S15). No obvious increase could be observed after 24 h of stirring, which indicated the aggregates state of IA-P25 remained relatively stable after 24 h. This result could correspond to the more stable H_2 rate of IA-P25-stirring. In order to elucidate if it is possible to get the steady state, a long-term photocatalytic experiment of IA-P25 (72 h) was performed (Fig. S16). We can observe that the hydrogen production rate is continuously decreasing, although it is becoming more stable with time, remaining relatively stable after 64 h. Combined with the PL results discussed above, it could be inferred that this relatively slow deactivation was no longer mainly attributed to the separation of aggregates, but to the combined effect of multiple factors such as the accumulation of intermediates. It was worth noting that the H_2 production rate of IAP25 at 72 h was still 1.5 times higher than that of P25 at 24 h, which was consistent with the results that IA-P25 always presented a relatively lower PL intensity. Interestingly, after ultrasound treatment, IA-P25 exhibited a similar PL spectrum as P25. All these results suggested that the recombination efficiency of charge carrier increased with the separation of aggregate, which was highly consistent with the results of H_2 production and the proposed mechanism.

4. Conclusions

Our results indicate that a simple filtration method can be used to create titania nanoparticle aggregations without introducing any relevant chemical modifications. This approach allowed us to easily determine the effect of the aggregation size on the photo-reforming of ethanol. When low loadings of Pt are used as co-catalyst, the formation of these aggregations dramatically improves the photocatalytic activity. As reference, the total hydrogen produced using 0.05 wt% of Pt and the IA-P25 is 6.2 times higher than that obtained using the raw P25 with the

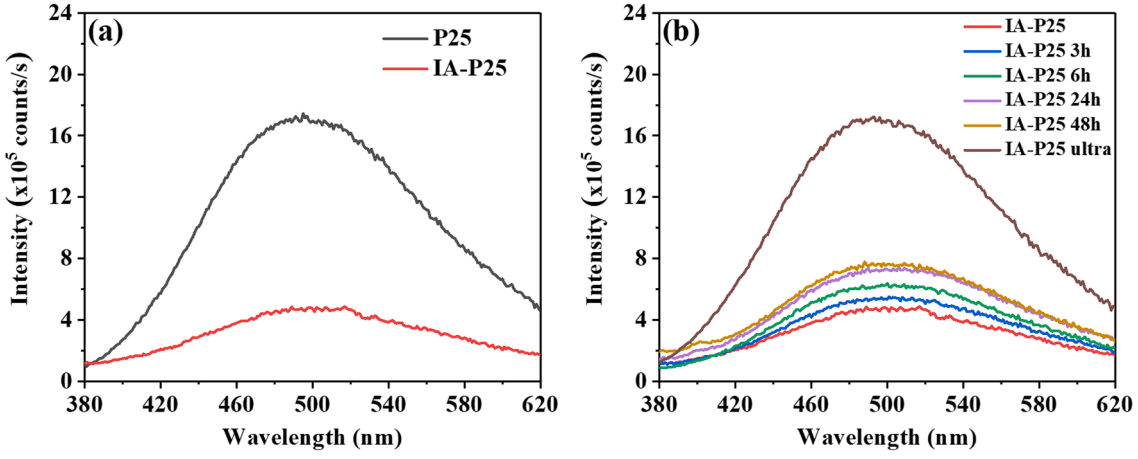

Fig. 9. (a) PL emission spectra of samples and (b) PL emission spectra of IA-P25 under different treatment conditions.

same platinum loading. Our findings lead us to conclude that the formation of titania nanoparticle aggregations promotes an interface that favors the mobility of the photo-generated charges between the nanoparticles decreasing the recombination rate. Therefore, the simple physical contact between the titania nanoparticles can create an efficient heterojunction as it was demonstrated by our fluorescence study in liquid phase. Thanks to this phenomenon, smaller amounts of Pt are needed to ensure a remarkable catalytic activity, as all the titania particles in the aggregate act as an antenna collecting the sun-light to obtain photo-generated electrons that will be transferred to the Pt nanoparticles where the reduction half-reaction will be catalyzed. The photodeposition of the platinum ensures that nanoparticles will decorate the areas of the support where the photo-excited electrons would accumulate in the aggregates. This information is also valuable if we consider that special efforts should be conducted to immobilize the photocatalysts in the case of future real applications, particularly in reactor designs. According to our results, the immobilization of semiconductor-cocatalyst is a low efficient strategy and a better approach would be to immobilize the semiconductor and subsequently photodeposit the cocatalyst.

Our findings underscore the critical importance of considering the degree of aggregation in photocatalyst materials when interpreting photocatalytic results. It's noteworthy that many photocatalyst synthesis processes involve similar filtration steps, which can potentially lead to inaccurate activity assessments. Furthermore, this impact may vary depending on the specific photocatalytic application. To ensure a precise determination of a material's intrinsic activity, we strongly encourage the inclusion of low-intensity ultrasound treatment in research methodologies. It's worth noting that this approach is often skipped in current research practices and may explain some of the apparent contradictions found in the literature. By including this step, we can enhance the reliability and comparability of photocatalytic studies, ultimately advancing our understanding of these critical materials.

CRediT authorship contribution statement

Enqi Bu: Writing – review & editing, Writing – original draft, Methodology, Investigation, Conceptualization. **Xiaowei Chen:** Writing – review & editing, Supervision, Project administration, Funding acquisition, Conceptualization. **Carlos López-Cartes:** Writing – review & editing, Investigation, Formal analysis. **Antonio Monzón:** Writing – review & editing, Funding acquisition. **Juan José Delgado:** Writing – review & editing, Writing – original draft, Supervision, Project administration, Methodology, Investigation, Funding acquisition, Formal analysis, Conceptualization.

Declaration of competing interest

The authors declare the following financial interests/personal relationships which may be considered as potential competing interests: Juan Jose Delgado reports financial support was provided by Spain Ministry of Science and Innovation and Junta de Andalucia. Antonio Monzon reports financial support was provided by Spain Ministry of Science and Innovation.

Data availability

Data will be made available on request.

Acknowledgement

Authors would like to thank the support by MINECO (Spain) through projects PID2020-113809RB-C31 and PID2020-113809RB-C33. E. Bu would also like to thank the University of Cadiz for FPI-UCA grant (UCA/R93REC/2019).

Appendix A. Supplementary data

Supplementary data to this article can be found online at https://doi.org/10.1016/j.jcis.2024.07.028.

References

[1] K.J. Dillman, J. Heinonen, A 'just' hydrogen economy: A normative energy justice assessment of the hydrogen economy, Renew. Sustain. Energy Rev. 167 (2022) 112648, https://doi.org/10.1016/j.rser.2022.112648.
[2] F. Qureshi, M. Yusuf, H. Kamyab, D.V.N. Vo, S. Chelliapan, S.W. Joo, Y. Vasseghian, Latest eco-friendly avenues on hydrogen production towards a circular bioeconomy: Currents challenges, innovative insights, and future perspectives, Renew. Sustain. Energy Rev. 168 (2022) 112916, https://doi.org/10.1016/j.rser.2022.112916.
[3] Z. Chen, F. Guo, H. Sun, Y. Shi, W. Shi, Well-designed three-dimensional hierarchical hollow tubular g-C_3N_4/$ZnIn_2S_4$ nanosheets heterostructure for achieving efficient visible-light photocatalytic hydrogen evolution, J. Colloid Interface Sci. 607 (2022) 1391–1401, https://doi.org/10.1016/j.jcis.2021.09.095.
[4] J. Yu, Y. Hai, M. Jaroniec, Photocatalytic hydrogen production over CuO-modified titania, J. Colloid Interface Sci. 357 (2011) 223–228, https://doi.org/10.1016/j.jcis.2011.01.101.
[5] T. Uekert, C.M. Pichler, T. Schubert, E. Reisner, Solar-driven reforming of solid waste for a sustainable future, Nat. Sustain. 4 (2021) 383–391, https://doi.org/10.1038/s41893-020-00650-x.
[6] B. Rico-Oller, A. Boudjemaa, H. Bahruji, M. Kebir, S. Prashar, K. Bachari, M. Fajardo, S. Gómez-Ruiz, Photodegradation of organic pollutants in water and green hydrogen production via methanol photoreforming of doped titanium oxide nanoparticles, Sci. Total Environ. 563–564 (2016) 921–932, https://doi.org/10.1016/j.scitotenv.2015.10.101.
[7] X. Zhang, L. Luo, R. Yun, M. Pu, B. Zhang, X. Xiang, Increasing the Activity and Selectivity of TiO_2-Supported Au Catalysts for Renewable Hydrogen Generation from Ethanol Photoreforming by Engineering Ti^{3+} Defects, ACS Sustain. Chem. Eng. 7 (2019) 13856–13864, https://doi.org/10.1021/acssuschemeng.9b02008.
[8] C. Wang, X. Cai, Y. Chen, Z. Cheng, X. Luo, S. Mo, L. Jia, P. Lin, Z. Yang, Improved hydrogen production from glycerol photoreforming over sol-gel derived TiO_2 coupled with metal oxides, Chem. Eng. J. 317 (2017) 522–532, https://doi.org/10.1016/j.cej.2017.02.033.
[9] L. Zhang, W. Wang, S. Zeng, Y. Su, H. Hao, Enhanced H_2 evolution from photocatalytic cellulose conversion based on graphitic carbon layers on TiO_2/NiO_x, Green Chem. 20 (2018) 3008–3013, https://doi.org/10.1039/c8gc01398e.
[10] H. Nagakawa, M. Nagata, Highly Efficient Hydrogen Production in the Photoreforming of Lignocellulosic Biomass Catalyzed by Cu, In-Doped ZnS Derived from ZIF-8, Adv. Mater. Interfaces. 9 (2021) 2101581, https://doi.org/10.1002/admi.202101581.
[11] C.R. López, E.P. Melián, J.A. Ortega Méndez, D.E. Santiago, J.M. Doña Rodríguez, O. González Díaz, Comparative study of alcohols as sacrificial agents in H_2 production by heterogeneous photocatalysis using Pt/TiO_2 catalysts, J. Photochem. Photobiol. A Chem. 312 (2015) 45–54, https://doi.org/10.1016/j.jphotochem.2015.07.005.
[12] A.V. Puga, Photocatalytic production of hydrogen from biomass-derived feedstocks, Coord. Chem. Rev. 315 (2016) 1–66, https://doi.org/10.1016/j.ccr.2015.12.009.
[13] C. Shi, M. Eqi, J. Shi, Z. Huang, H. Qi, Constructing 3D hierarchical TiO_2 microspheres with enhanced mass diffusion for efficient glucose photoreforming under modulated reaction conditions, J. Colloid Interface Sci. 650 (2023) 1736–1748, https://doi.org/10.1016/j.jcis.2023.07.081.
[14] B. Ohtani, O.O. Prieto-Mahaney, D. Li, R. Abe, What is Degussa (Evonic) P25? Crystalline composition analysis, reconstruction from isolated pure particles and photocatalytic activity test, J. Photochem. Photobiol. A Chem. 216 (2010) 179–182, https://doi.org/10.1016/j.jphotochem.2010.07.024.
[15] K. Woan, G. Pyrgiotakis, W. Sigmund, Photocatalytic carbon-nanotube-TiO_2 composites, Adv. Mater. 21 (2009) 2233–2239, https://doi.org/10.1002/adma.200802738.
[16] X. Yue, J. Hou, H. Zhao, P. Wu, Y. Guo, Q. Shi, L. Chen, S. Peng, Z. Liu, G. Cao, Au–Ag alloy nanoparticles with tunable cavity for plasmon-enhanced photocatalytic H_2 evolution, J. Energy Chem. 49 (2020) 1–7, https://doi.org/10.1016/j.jechem.2020.01.005.
[17] C. Marchal, T. Cottineau, M.G. Méndez-Medrano, C. Colbeau-Justin, V. Caps, V. Keller, Au/TiO_2–gC_3N_4 Nanocomposites for Enhanced Photocatalytic H_2 Production from Water under Visible Light Irradiation with Very Low Quantities of Sacrificial Agents, Adv. Energy Mater. 8 (2018) 1702142, https://doi.org/10.1002/aenm.201702142.
[18] P. Jiménez-Calvo, V. Caps, M.N. Ghazzal, C. Colbeau-Justin, V. Keller, Au/TiO_2(P25)-gC_3N_4 composites with low gC_3N_4 content enhance TiO_2 sensitization for remarkable H_2 production from water under visible-light irradiation, Nano Energy 75 (2020) 104888, https://doi.org/10.1016/j.nanoen.2020.104888.
[19] H. Zhao, X. Yu, C.F. Li, W. Yu, A. Wang, Z.Y. Hu, S. Larter, Y. Li, M. Golam Kibria, J. Hu, Carbon quantum dots modified TiO_2 composites for hydrogen production and selective glucose photoreforming, J. Energy Chem. 64 (2022) 201–208, https://doi.org/10.1016/j.jechem.2021.04.033.
[20] M. Bellardita, E.I. García-López, G. Marcì, L. Palmisano, Photocatalytic formation of H_2 and value-added chemicals in aqueous glucose (Pt)-TiO_2 suspension, Int. J.

Hydrogen Energy. 41 (2016) 5934–5947, https://doi.org/10.1016/j.ijhydene.2016.02.103.
[21] Y. Cho, S. Kim, B. Park, C.L. Lee, J.K. Kim, K.S. Lee, I.Y. Choi, J.K. Kim, K. Zhang, S. H. Oh, J.H. Park, Multiple Heterojunction in Single Titanium Dioxide Nanoparticles for Novel Metal-Free Photocatalysis, Nano Lett. 18 (2018) 4257–4262, https://doi.org/10.1021/acs.nanolett.8b01245.
[22] K. Gao, H. Guo, Y. Hu, H. He, M. Li, X. Gao, F. Fu, Accurate design of spatially separated double active site in Bi_4NbO_8Cl single crystal to promote Z - Scheme photocatalytic overall water splitting, J. Energy Chem. 87 (2023) 568–582, https://doi.org/10.1016/j.jechem.2023.08.038.
[23] G.M. Haselmann, D. Eder, Early-Stage Deactivation of Platinum-Loaded TiO_2 Using in Situ Photodeposition during Photocatalytic Hydrogen Evolution, ACS Catal. 7 (2017) 4668–4675, https://doi.org/10.1021/acscatal.7b00845.
[24] H.A. Vignolo-González, S. Laha, A. Jiménez-Solano, T. Oshima, V. Duppel, P. Schützendübe, B.V. Lotsch, Toward Standardized Photocatalytic Oxygen Evolution Rates Using RuO_2@TiO_2 as a Benchmark, Matter. 3 (2020) 464–486, https://doi.org/10.1016/j.matt.2020.07.021.
[25] R.I. Bickley, T. Gonzalez-Carreno, J.S. Lees, L. Palmisano, R.J.D. Tilley, A structural investigation of titanium dioxide photocatalysts, J. Solid State Chem. 92 (1991) 178–190, https://doi.org/10.1016/0022-4596(91)90255-G.
[26] D.C. Hurum, A.G. Agrios, K.A. Gray, T. Rajh, M.C. Thurnauer, Explaining the enhanced photocatalytic activity of Degussa P25 mixed-phase TiO_2 using EPR, J. Phys. Chem. B. 107 (2003) 4545–4549, https://doi.org/10.1021/jp0273934.
[27] A.V. Emeline, L.G. Smirnova, G.N. Kuzmin, L.L. Basov, N. Serpone, Spectral dependence of quantum yields in gas-solid heterogeneous photosystems. Influence of anatase/rutile content on the photostimulated adsorption of dioxygen and dihydrogen on titania, J. Photochem. Photobiol. A Chem. 148 (2002) 97–102, https://doi.org/10.1016/S1010-6030(02)00078-3.
[28] G.L. Chiarello, M.V. Dozzi, E. Selli, TiO_2-based materials for photocatalytic hydrogen production, J. Energy Chem. 26 (2017) 250–258, https://doi.org/10.1016/j.jechem.2017.02.005.
[29] M. Dahl, Y. Liu, Y. Yin, Composite titanium dioxide nanomaterials, Chem. Rev. 114 (2014) 9853–9889, https://doi.org/10.1021/cr400634p.
[30] Y. Shu, J. Ji, M. Zhou, S. Liang, Q. Xie, S. Li, B. Liu, J. Deng, J. Cao, S. Liu, H. Huang, Selective photocatalytic oxidation of gaseous ammonia at ppb level over Pt and F modified TiO_2, Appl. Catal. B Environ. 300 (2022) 120688, https://doi.org/10.1016/j.apcatb.2021.120688.
[31] Y. Liu, Z. Sun, Y.H. Hu, Bimetallic cocatalysts for photocatalytic hydrogen production from water, Chem. Eng. J. 409 (2021) 128250, https://doi.org/10.1016/j.cej.2020.128250.
[32] L.Y. Lin, S. Kavadiya, X. He, W.N. Wang, B.B. Karakocak, Y.C. Lin, M.Y. Berezin, P. Biswas, Engineering stable Pt nanoparticles and oxygen vacancies on defective TiO_2 via introducing strong electronic metal-support interaction for efficient CO_2 photoreduction, Chem. Eng. J. 389 (2020) 123450, https://doi.org/10.1016/j.cej.2019.123450.
[33] D. Yazaki, T. Kawawaki, D. Hirayama, M. Kawachi, K. Kato, S. Oguchi, Y. Yamaguchi, S. Kikkawa, Y. Ueki, S. Hossain, D.J. Osborn, F. Ozaki, S. Tanaka, J. Yoshinobu, G.F. Metha, S. Yamazoe, A. Kudo, A. Yamakata, Y. Negishi, Carbon Nitride Loaded with an Ultrafine, Monodisperse, Metallic Platinum-Cluster Cocatalyst for the Photocatalytic Hydrogen-Evolution Reaction, Small 19 (2023) 2208287, https://doi.org/10.1002/smll.202208287.
[34] S. Nakabayashi, A. Fujishima, K. Honda, Experimental evidence for the hydrogen evolution site in photocatalytic process on Pt/TiO_2, Chem. Phys. Lett. 102 (1983) 464–465, https://doi.org/10.1016/0009-2614(83)87447-8.
[35] R. Li, F. Zhang, D. Wang, J. Yang, M. Li, J. Zhu, X. Zhou, H. Han, C. Li, Spatial separation of photogenerated electrons and holes among 010 and 110 crystal facets of BiVO4, Nat. Commun. 4 (2013) 1432, https://doi.org/10.1038/ncomms2401.
[36] E. Bu, X. Chen, C. López-Cartes, F. Cazaña, A. Monzón, J. Martínez-López, J. J. Delgado, Effect of the TiO_2-carbon interface on charge transfer and ethanol photo-reforming, Catal. Today. 422 (2023) 114220, https://doi.org/10.1016/j.cattod.2023.114220.
[37] D.Y.C. Leung, X. Fu, C. Wang, M. Ni, M.K.H. Leung, X. Wang, X. Fu, Hydrogen production over titania-based photocatalysts, ChemSusChem 3 (2010) 681–694, https://doi.org/10.1002/cssc.201000014.
[38] M.C. Biesinger, L.W.M. Lau, A.R. Gerson, R.S.C. Smart, Resolving surface chemical states in XPS analysis of first row transition metals, oxides and hydroxides: Sc, Ti, V, Cu and Zn, Appl. Surf. Sci. 257 (2010) 887–898, https://doi.org/10.1016/j.apsusc.2010.07.086.
[39] W. Yuan, P. Yuan, D. Liu, W. Yu, M. Laipan, L. Deng, F. Chen, In situ hydrothermal synthesis of a novel hierarchically porous TS-1/modified-diatomite composite for methylene blue (MB) removal by the synergistic effect of adsorption and photocatalysis, J. Colloid Interface Sci. 462 (2016) 191–199, https://doi.org/10.1016/j.jcis.2015.09.067.
[40] J. Xiong, Q. Wu, X. Mei, J. Liu, Y. Wei, Z. Zhao, D. Wu, J. Li, Fabrication of Spinel-Type $Pd_xCo_{3-x}O_4$ Binary Active Sites on 3D Ordered Meso-macroporous Ce-Zr-O_2 with Enhanced Activity for Catalytic Soot Oxidation, ACS Catal. 8 (2018) 7915–7930, https://doi.org/10.1021/acscatal.8b01924.
[41] L. Wang, S. Duan, P. Jin, H. She, J. Huang, Z. Lei, T. Zhang, Q. Wang, Anchored Cu (II) tetra(4-carboxylphenyl)porphyrin to P25 (TiO_2) for efficient photocatalytic ability in CO_2 reduction, Appl. Catal. B Environ. 239 (2018) 599–608, https://doi.org/10.1016/j.apcatb.2018.08.007.
[42] J. Yu, H. Yu, B. Cheng, M. Zhou, X. Zhao, Enhanced photocatalytic activity of TiO_2 powder (P25) by hydrothermal treatment, J. Mol. Catal. A Chem. 253 (2006) 112–118, https://doi.org/10.1016/j.molcata.2006.03.021.
[43] L. Al-Gebory, M.P. Mengüç, The effect of pH on particle agglomeration and optical properties of nanoparticle suspensions, J. Quant. Spectrosc. Radiat. Transf. 219 (2018) 46–60, https://doi.org/10.1016/j.jqsrt.2018.07.020.
[44] L.Y. Kunz, J. Hong, A.R. Riscoe, A. Majumdar, M. Cargnello, Reducing instability in dispersed powder photocatalysis derived from variable dispersion, metallic co-catalyst morphology, and light fluctuations, J. Photochem. Photobiol. 2 (2020) 100004, https://doi.org/10.1016/j.jpap.2020.100004.
[45] Y. Shiraishi, H. Hirakawa, Y. Togawa, Y. Sugano, S. Ichikawa, T. Hirai, Rutile crystallites isolated from degussa (Evonik) P25 TiO_2: Highly efficient photocatalyst for chemoselective hydrogenation of nitroaromatics, ACS Catal. 3 (2013) 2318–2326, https://doi.org/10.1021/cs400532p.
[46] A.C. Sola, N. Homs, P. Ramírez de la Piscina, Photocatalytic H_2 production from ethanol (aq) solutions: The effect of intermediate products, Int. J. Hydrogen Energy. 41 (2016) 19629–19636, https://doi.org/10.1016/j.ijhydene.2016.05.268.
[47] A.V. Puga, A. Forneli, H. García, A. Corma, Production of H_2 by ethanol photoreforming on Au/TiO_2, Adv. Funct. Mater. 24 (2014) 241–248, https://doi.org/10.1002/adfm.201301907.
[48] H. Huang, J. Feng, S. Zhang, H. Zhang, X. Wang, T. Yu, C. Chen, Z. Yi, J. Ye, Z. Li, Z. Zou, Molecular-level understanding of the deactivation pathways during methanol photo-reforming on Pt-decorated TiO_2, Appl. Catal. B Environ. 272 (2020) 118980, https://doi.org/10.1016/j.apcatb.2020.118980.
[49] G.M. Haselmann, B. Baumgartner, J. Wang, K. Wieland, T. Gupta, C. Herzig, A. Limbeck, B. Lendl, D. Eder, In Situ Pt Photodeposition and Methanol Photooxidation on Pt/TiO_2: Pt-Loading-Dependent Photocatalytic Reaction Pathways Studied by Liquid-Phase Infrared Spectroscopy, ACS Catal. 10 (2020) 2964–2977, https://doi.org/10.1021/acscatal.9b05588.
[50] D. Wang, Z.P. Liu, W.M. Yang, Revealing the Size Effect of Platinum Cocatalyst for Photocatalytic Hydrogen Evolution on TiO_2 Support: A DFT Study, ACS Catal. 8 (2018) 7270–7278, https://doi.org/10.1021/acscatal.8b01886.
[51] J. Yan, X. Li, S. Yang, X. Wang, W. Zhou, Y. Fang, S. Zhang, F. Peng, S. Zhang, Design and preparation of CdS/H-3D-TiO_2/Pt-wire photocatalysis system with enhanced visible-light driven H_2 evolution, Int. J. Hydrogen Energy. 42 (2017) 928–937, https://doi.org/10.1016/j.ijhydene.2016.08.188.
[52] F. Gärtner, S. Losse, A. Boddien, M.M. Pohl, S. Denurra, H. Junge, M. Beller, Hydrogen evolution from water/alcohol mixtures: Effective in situ generation of an active Au/TiO_2 catalyst, ChemSusChem 5 (2012) 530–533, https://doi.org/10.1002/cssc.201100281.
[53] M. Bellardita, H.A.E. Nazer, V. Loddo, F. Parrino, A.M. Venezia, L. Palmisano, Photoactivity under visible light of metal loaded TiO_2 catalysts prepared by low frequency ultrasound treatment, Catal. Today. 284 (2017) 92–99, https://doi.org/10.1016/j.cattod.2016.11.026.
[54] P.A. Osorio-Vargas, C. Pulgarin, A. Sienkiewicz, L.R. Pizzio, M.N. Blanco, R. A. Torres-Palma, C. Pétrier, J.A. Rengifo-Herrera, Low-frequency ultrasound induces oxygen vacancies formation and visible light absorption in TiO_2 P-25 nanoparticles, Ultrason. Sonochem. 19 (2012) 383–386, https://doi.org/10.1016/j.ultsonch.2011.11.013.
[55] A. Houas, H. Lachheb, M. Ksibi, E. Elaloui, C. Guillard, J.M. Herrmann, Photocatalytic degradation pathway of methylene blue in water, Appl. Catal. B Environ. 31 (2001) 145–157, https://doi.org/10.1016/S0926-3373(00)00276-9.
[56] X. Yuan, D. Dragoe, P. Beaunier, D.B. Uribe, L. Ramos, M.G. Méndez-Medrano, H. Remita, Polypyrrole nanostructures modified with mono- and bimetallic nanoparticles for photocatalytic H_2 generation, J. Mater. Chem. a. 8 (2020) 268–277, https://doi.org/10.1039/c9ta11088g.
[57] F. Wang, R.J. Wong, J.H. Ho, Y. Jiang, R. Amal, Sensitization of Pt/TiO_2 Using Plasmonic Au Nanoparticles for Hydrogen Evolution under Visible-Light Irradiation, ACS Appl. Mater. Interfaces. 9 (2017) 30575–30582, https://doi.org/10.1021/acsami.7b06265.
[58] K.E. Sanwald, T.F. Berto, W. Eisenreich, A. Jentys, O.Y. Gutiérrez, J.A. Lercher, Overcoming the Rate-Limiting Reaction during Photoreforming of Sugar Aldoses for H_2-Generation, ACS Catal. 7 (2017) 3236–3244, https://doi.org/10.1021/acscatal.7b00508.
[59] S. Qin, J. Will, H. Kim, N. Denisov, S. Carl, E. Spiecker, P. Schmuki, Single Atoms in Photocatalysis: Low Loading Is Good Enough!, ACS Energy Lett. 8 (2023) 1209–1214, https://doi.org/10.1021/acsenergylett.2c02801.
[60] M.J. Elser, T. Berger, D. Brandhuber, J. Bernardi, O. Diwald, E. Knözinger, Particles coming together: Electron centers in adjoined TiO_2 nanocrystals, J. Phys. Chem. B. 110 (2006) 7605–7608, https://doi.org/10.1021/jp0607465.
[61] P. Li, X. Yan, S. Gao, R. Cao, Boosting photocatalytic hydrogen production coupled with benzyl alcohol oxidation over CdS/metal–organic framework composites, Chem. Eng. J. 421 (2021) 129870, https://doi.org/10.1016/j.cej.2021.129870.
[62] C. Wu, Z. Gao, S. Gao, Q. Wang, H. Xu, Z. Wang, B. Huang, Y. Dai, Ti^{3+} self-doped TiO_2 photoelectrodes for photoelectrochemical water splitting and photoelectrocatalytic pollutant degradation, J. Energy Chem. 25 (2016) 726–733, https://doi.org/10.1016/j.jechem.2016.04.009.
[63] J. Serafin, M. Ouzzine, J. Sreńscek-Nazzal, J. Llorca, Photocatalytic hydrogen production from alcohol aqueous solutions over TiO_2-activated carbon composites decorated with Au and Pt, J. Photochem. Photobiol. A Chem. 425 (2022) 113726, https://doi.org/10.1016/j.jphotochem.2021.113726.
[64] H. Jiang, H. Chen, Y. Fu, C. Guo, $SnFe_2O_4$ mediated near-infrared-driven photocatalysis, photothermal sterilization and piezocatalysis, Appl. Surf. Sci. 611 (2023) 155555, https://doi.org/10.1016/j.apsusc.2022.155555.
[65] J. Niu, J. Albero, P. Atienzar, H. García, Porous Single-Crystal-Based Inorganic Semiconductor Photocatalysts for Energy Production and Environmental

Remediation: Preparation, Modification, and Applications, Adv. Funct. Mater. 30 (2020) 1908984, https://doi.org/10.1002/adfm.201908984.

[66] L. Jing, Y. Qu, B. Wang, S. Li, B. Jiang, L. Yang, W. Fu, H. Fu, J. Sun, Review of photoluminescence performance of nano-sized semiconductor materials and its relationships with photocatalytic activity, Sol. Energy Mater. Sol. Cells. 90 (2006) 1773–1787, https://doi.org/10.1016/J.SOLMAT.2005.11.007.

[67] L. Zhang, C.G. Niu, X.J. Wen, H. Guo, X.F. Zhao, C. Liang, G.M. Zeng, Enhanced photocatalytic activity of CdS/SnS_2 nanocomposite with highly-efficient charge transfer and visible light utilization for selective reduction of 4-nitroaniline, J. Colloid Interface Sci. 532 (2018) 557–570, https://doi.org/10.1016/j.jcis.2018.08.017.